geotechnics

MDPI

Article

Dynamic Axial Pile Stiffness and Damping in Soil with Double Inhomogeneity

Konstantinos Syngros [1] and George Mylonakis [2,3,*]

[1] Langan Engineering, 368 9th Avenue, New York, NY 10001, USA; ksyngros@langan.com
[2] Department of Civil and Environmental Engineering, Khalifa University, Abu Dhabi P.O. Box 127788, United Arab Emirates
[3] School of Civil, Aerospace and Design Engineering University of Bristol, Queen's Building, University Walk, Bristol BS8 1TR, UK
* Correspondence: george.mylonakis@ku.ac.ae or g.mylonakis@bristol.ac.uk

Abstract

Viscoelastic solutions are developed for the axial dynamic response of single piles in soil profiles that are inhomogeneous both vertically (with depth) and horizontally (with radial distance from the pile). While vertical soil inhomogeneity has been well explored, horizontal inhomogeneity has received limited research attention. In this work, the problem is treated in the realm of linear elastodynamic theory by employing a rigorous finite-element formulation specifically developed by the authors for the problem at hand. The effect of double soil inhomogeneity is investigated with reference to: (1) pile head stiffness; (2) pile-head radiation damping; (3) soil reaction along the pile; and (4) variation of the above with loading frequency. To this end, four different soil profiles are considered in conjunction with different levels of soil inhomogeneity, pile lengths, pile–soil stiffness contrasts, and boundary conditions at the pile tip. It is shown that the effect of inhomogeneity has unique features that cannot be captured by using a substitute homogeneous profile. Modeling an inhomogeneous soil as a homogeneous layer providing equal pile-head stiffness (to be referred in this work to as "stiffness-equivalent soil") may grossly overestimate wave radiation, leading to dampened estimates of dynamic pile response. Simulations of two field experiments are reported, and implications of radiation damping in design are discussed.

Keywords: pile; dynamics; soil inhomogeneity; radiation damping; numerical analysis; finite elements

Check for updates

Academic Editor: Grigorios Tsinidis

Received: 16 January 2026
Revised: 9 March 2026
Accepted: 11 March 2026
Published: 19 March 2026

Copyright: © 2026 by the authors. Licensee MDPI, Basel, Switzerland. This article is an open access article distributed under the terms and conditions of the Creative Commons Attribution (CC BY) license.

1. Introduction

Piles during earthquake shaking are subjected to loads at their top generated by the inertia of the oscillating superstructure (inertial loading) as well as additional loads imposed along their length by the deforming soil, which develops regardless of the presence of a superstructure (kinematic loading) [1–11]. An important associated phenomenon is the beneficial role of piles in reducing the dynamic foundation input motion which has been studied in relation to both translational [12,13] and rotational excitation components [14]. It is known in this regard that the fundamental parameter regulating the importance of the kinematically induced rotation is pile axial stiffness.

With reference to axial pile response, early works [15,16] consider the fundamental problem of static loading and homogeneous soil. More complex cases involving steady-state dynamic loading [17,18] and inhomogeneous soil were treated by subsequent investigators [19–27]. State-of-the-art reviews have been presented, among oth-

ers, by Poulos [28], Novak [29], Pender [30], Gazetas & Mylonakis [31], Randolph [32], Crispin and Mylonakis [33], and Di Laora and Rovithis [34]. In most studies, the supporting soil is treated as either homogeneous or layered with constant material properties in each layer (e.g., Kaynia & Kausel [21]). A more realistic assumption is that of combined vertical and horizontal soil inhomogeneity. Vertical inhomogeneity is a typical geotechnical characteristic generated by sedimentation, overburden and over-consolidation. On the other hand, horizontal inhomogeneity is less recognized, generated by the softening/loosening of soil material in the vicinity of the pile caused by installation (i.e., driving or drilling) and post-installation loading [35,36]. This paper recognizes that the effect of soil inhomogeneity has certain unique characteristics that cannot be captured by using a substitute homogeneous profile. Only a handful of studies consider the effect of radial soil inhomogeneity, mostly through simplified plane-strain models under the assumption of vertically homogeneous or layered soil [36–42]. More recently, authors used rigorous methods to investigate specific construction-related effects in the response of piles (for example, [43,44]). To the extent of the authors' knowledge, no systematic investigations by rigorous computational means of the effect of combined vertical and horizontal soil inhomogeneity on dynamic pile response are available to date. Important unexplored topics include: (1) effect of combined inhomogeneity on static pile stiffness, (2) variation of pile stiffness and damping with loading frequency, (3) reduction in radiation damping with increasing inhomogeneity, and (4) effect of inhomogeneity on dynamic soil reaction along the pile. This gap in knowledge provided the motivation for the herein reported work.

2. Problem Definition and Model Development

The system considered is depicted in Figure 1: a vertical solid cylindrical pile embedded in inhomogeneous viscoelastic soil layer over rigid or elastic bedrock, subjected to axial harmonic head loading. Perfect bonding (i.e., no gap or slippage) is assumed to exist between pile and soil. To analyze the problem, a finite-element (FE) solution is adopted, building upon earlier work by Blaney et al. [20], implemented through a computer program (K-PAX) specifically developed by the Authors for the problem at hand [45]. Special attention is paid to modeling soil inhomogeneity to properly capture its effect on pile response, as discussed below.

For modeling the pile and surrounding soil, quadratic isoparametric triangular finite elements are employed in axisymmetric mode, which allows a three-dimensional geometry to be modeled using two-dimensional elements. Use of equivalent three-dimensional solid elements, instead of one-dimensional beam elements for the pile, allows for incorporating Poisson effects and associated radial displacements at the soil–pile interface [46]. Linear variation of elastic modulus within the soil elements is considered to minimize stiffness discontinuities (and thereby spurious wave reflections) between neighboring elements. Other special features developed as part of this study include: (1) special infinite elements and transmitting boundaries at the edges of the mesh to realistically and efficiently represent the unbounded outer medium, following the approaches of Marques & Owen [47] and Kellezi [48]; (2) relatively small mesh (i.e., involving less than about 10^3 elements) made possible by exploiting the advantages of axisymmetric analysis and variable element size (Figure 1); and (3) novel integration algorithms to address singularities in element stiffness close to the axis of symmetry. The adopted integration scheme follows the stencil developed by Price [49]. Sensitivity analyses were performed by increasing the height (H) and width (S) of the mesh and using various mesh-refinement patterns to check the stability of the numerical solution. Additional discussion on numerical aspects of the work is provided in Syngros [45] and Syngros et al. [50].

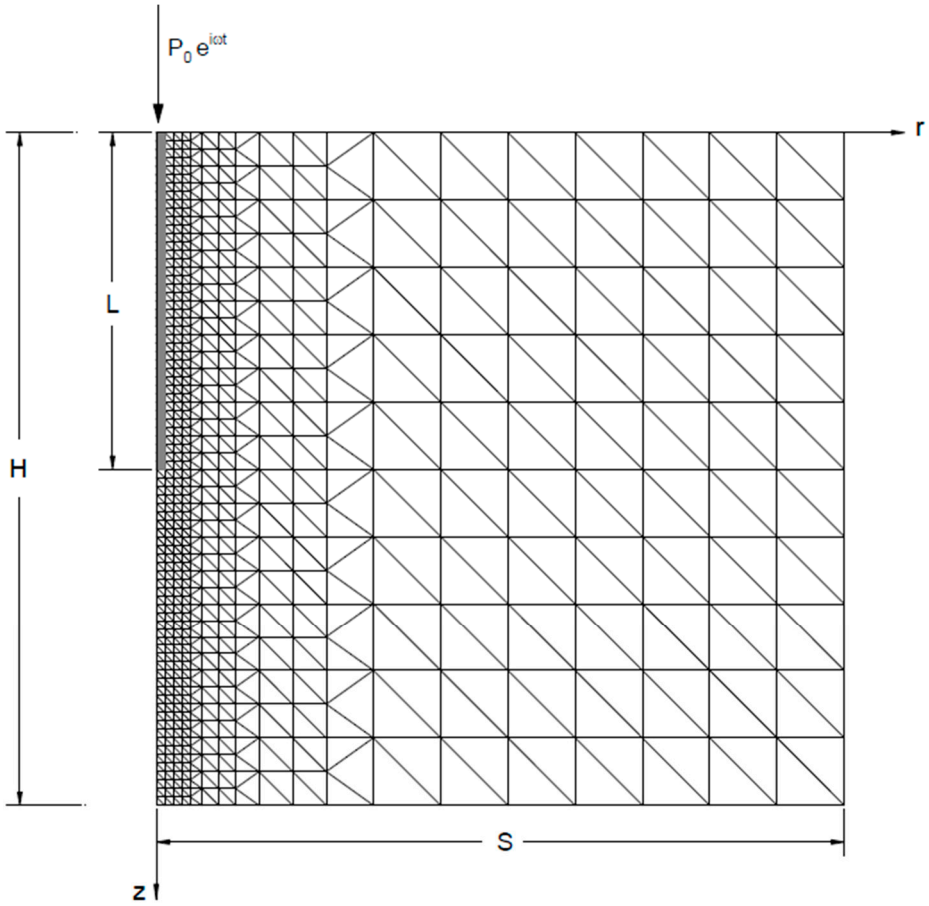


Figure 1. Typical axisymmetric finite element mesh for the problem under consideration. In the graph: H = mesh height, L = pile length, S = mesh width, r = radial distance from pile center line, z = depth. Elements shown in hatch represent the pile.

Modeling of Radial Soil Inhomogeneity

In their pioneering study, Novak & Sheta [37] model radial soil inhomogeneity around a pile using a plane-strain assumption that furnishes a configuration composed of two zones: (1) an inner ring of reduced elastic properties ("near-field") and (2) an outer ring of constant properties extending to infinity ("far-field"). This formulation introduces a discontinuity in stiffness at the boundary of the two zones, making the results sensitive to both frequency and ring radius. To prevent wave reflections at the discontinuity, Novak & Sheta consider the inner ring to be massless. In later studies, Veletsos & Dotson [38], Kim [51] and Bateman et al. [42,43] introduce more accurate transitions of elastic soil properties to the far-field by means of multiple concentric rings having increasing shear moduli and realistic mass, while boundary effects have been considered by Karatzia et al. [43] and Zheng et al. [52] in two and three dimensions, respectively. Also, Han & Sabin [39], Michaelides et al. [40] and El Naggar [41] considered continuous transition of elastic soil properties with radial distance from the pile and derived closed-form solutions to the plane-strain problem. The above solutions provided a simple practical framework for modeling radial inhomogeneity in the soil around a pile. Yet, because of the simplified underlying assumptions, their solutions neglect the continuity of the medium in the vertical direction and the stiffness mismatch between pile and soil, while under-predicting pile stiffness at low frequencies and lacking a cut-off frequency [1,29]. The proposed solution overcomes the above limitations.

Following Michaelides et al. [40], the simplified expression of Equation (1) is adopted here to model the variation of soil Young's modulus (E_s) with radial distance from pile centerline:

$$\frac{E_s(r)}{E_{s\infty}} = 1 - \left\{ A \frac{d}{2r} \right\}^n \quad (1)$$

in which $E_s(r)$ = soil modulus at radial distance r, $E_{s\infty}$ = soil modulus at infinity (practically at a radial distance greater than about 4 to 5 pile diameters), d = pile diameter, and A and n are dimensionless inhomogeneity parameters used to model the effect of pile-installation on the soil modulus. Evidently, at infinity, $E_s = E_{s\infty}$; at the pile–soil interface, $E_s(d/2) = (1 - A^n)\, E_{s\infty}$. To the authors' knowledge there is not a consolidated formulation that can address the change of Young's modulus with radial distance. That change would be dependent on type of pile, installation method, type of soil or rock, interface of pile and surrounding medium, and level of strain in the medium. The proposed formulation is generic, based on observations discussed in Reference [40].

Figure 2 shows normalized plots of $E_s(r)$ obtained from Equation (1), for a range of A and n values. It is observed that $E_s(r)$ varies rapidly in the immediate vicinity of the pile and approaches asymptotically the far-field value $E_{s\infty}$ at distances (r/d) greater than approximately 4. In the present study, the values A = 0, 0.1, 0.5 and 0.8 are adopted, pertaining to zero, low, medium and high levels of radial inhomogeneity in the near-pile soil. As shown in Figure 2, these values yield soil moduli at the pile–soil interface of about 100%, 80%, 40% and 15% of the far-field modulus, respectively. As will be demonstrated in the ensuing, using the generic value A = 0.8 in the finite element simulations and the empirical stiffness equations yields realistic displacements that agree with a broad set of field data from dynamic pile load tests. Further, the inhomogeneity coefficient n is generally of lesser importance, as evident in Figure 2. For simplicity and as a first approximation, n will be assumed here equal to 3/4 [40,45]. The main conclusions of this study are not affected by the exact value of n.

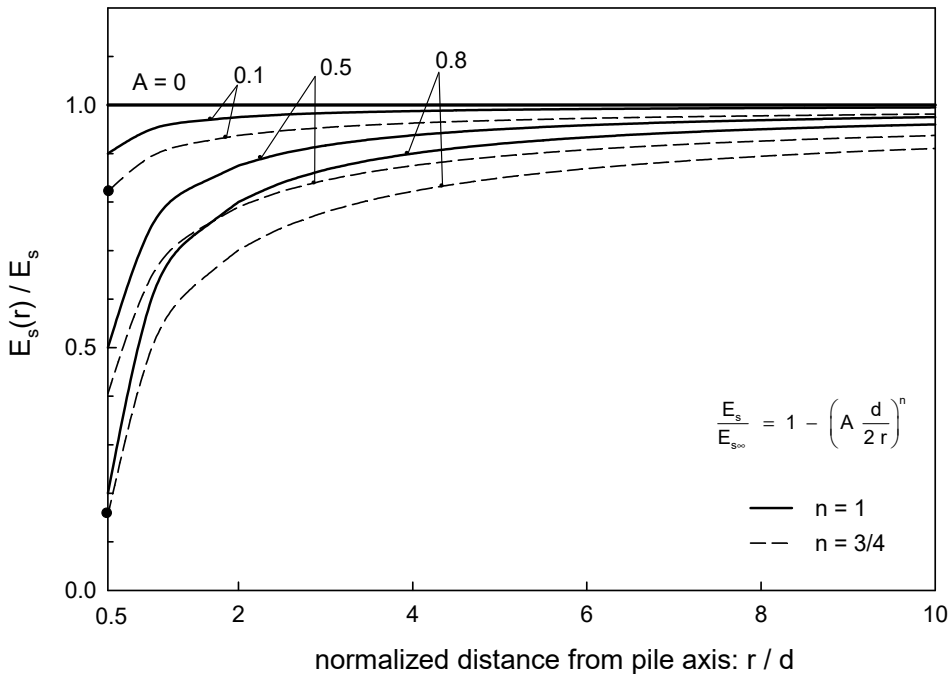


Figure 2. Variation of soil Young's modulus with radial distance from pile axis, for different soil inhomogeneity levels.

3. Soil and Pile Properties Considered

To examine a sufficient set of configurations, four different soil profiles are considered in the following, as shown in Figure 3.

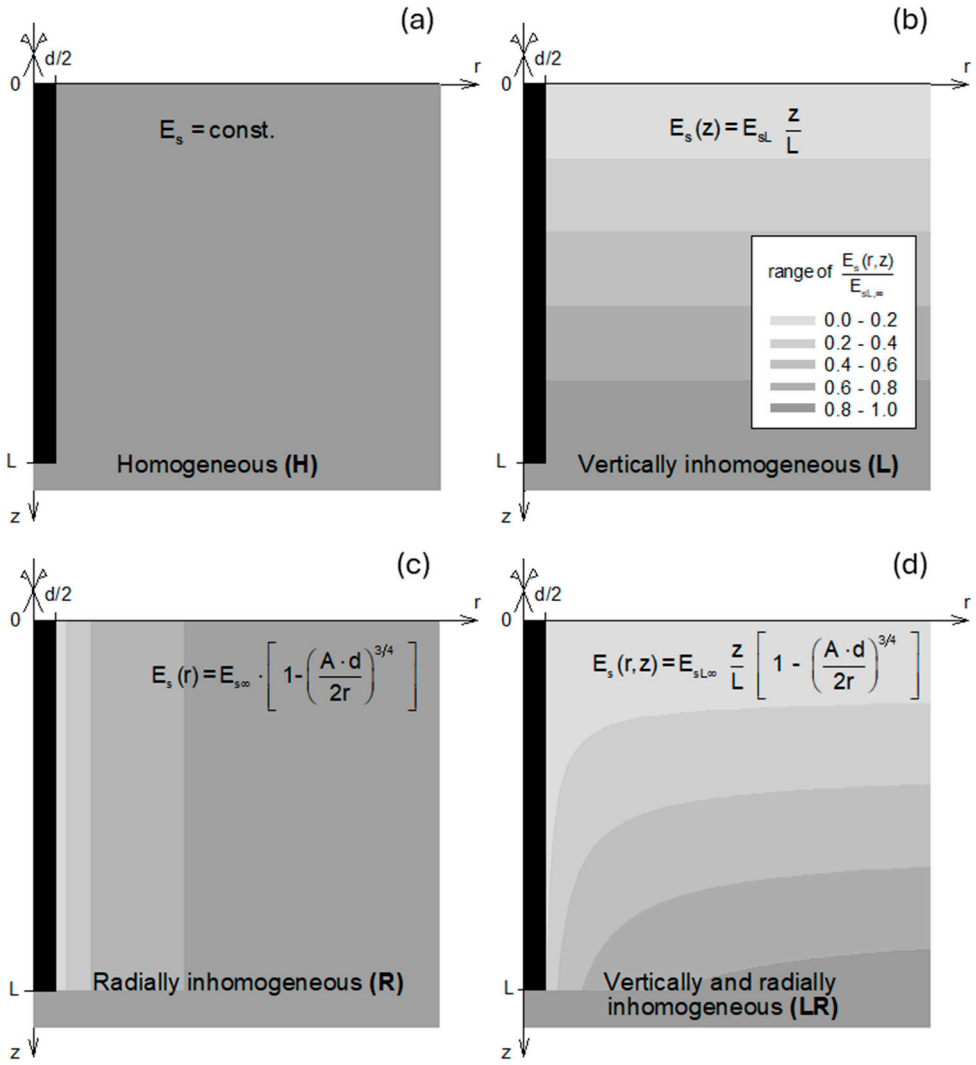


Figure 3. Variation in soil Young's modulus considered: Homogeneous, E_s (**a**); Linear with soil modulus at pile tip E_{sL} (**b**); Radial with soil modulus at infinity $E_{s\infty}$ (**c**); Linear–Radial with soil modulus at pile tip and infinity $E_{sL\infty}$ (**d**).

1. A reference homogeneous profile of constant modulus of elasticity described by

$$E_s(r,z) = E_s \tag{2}$$

2. A profile described by a modulus of elasticity increasing linearly with depth (to be referred hereafter to as "Linear" profile), starting from zero at the top and reaching E_{sL} at pile tip ($z = L$), then remaining constant, i.e.,

$$E_s(r,z) = E_s(z) = \begin{cases} E_{sL}\frac{z}{L} & , \ 0 \le z \le L \\ E_{sL} & , \ z > L \end{cases} \tag{3}$$

3. A profile whose modulus of elasticity is constant with depth but varies with radial distance from the pile (to be termed hereafter "Radial" profile), starting from a near-pile value $E_s(d/2)$ and increasing monotonically until it asymptotes to a far-field value of E_s according to Equation (1). As in the previous case, the soil is considered homogeneous below the pile tip. Accordingly,

$$E_s(r,z) = E_s(r) = \begin{cases} E_{sL\infty}\left[1 - \left(\frac{Ad}{2r}\right)^{3/4}\right], & z \le L \text{ and } r \ge d/2 \\ E_{sL\infty}, & z > L \end{cases} \quad (4)$$

4. A profile that is inhomogeneous in both the vertical and radial direction (to be referred hereafter to as "Linear-Radial" profile), whose modulus of elasticity varies linearly with depth above the pile tip ($z < L$) and with radial distance from the pile according to Equation (1). This is essentially a combination of the Linear and Radial profiles presented above and is characterized by a modulus $E_{sL\infty}$ at the depth of the pile tip and an infinite radial distance from the pile. In the same spirit as in the other profiles, Young's modulus below the pile tip is considered constant, equal to $E_{sL\infty}$.

$$E_s(r,z) = \begin{cases} E_{sL\infty}\frac{z}{L}\left[1 - \left(\frac{Ad}{2r}\right)^{3/4}\right], & z \le L \text{ and } r \ge d/2 \\ E_{sL\infty}, & z > L \end{cases} \quad (5)$$

Note that for $A = 0$, profile 4 duly reduces to the Linear profile in Equation (3) and profile 3 to the Homogeneous profile in Equation (2).

It should be stressed that use of equal reference moduli in the four soil profiles (i.e., $E_s = E_{sL} = E_{s\infty} = E_{sL\infty}$) furnishes models with very different stiffness (the homogeneous soil profile being the stiffest and the linear radial the softest), complicating comparisons of pile response under equal head loads. The issue will be discussed in more detail later in this article.

With reference to the pile–soil interacting system, the following parameters were considered: (1) dimensionless pile length (L/d) ranging from 10 (short pile) to 60 (slender pile); (2) pile–soil stiffness contrast (E_p/E_s) ranging from 20 (pile in stiff soil) to 10,000 (pile in soft soil); (3) Poisson's ratio $\nu_s = 0.4$ for the soil and $\nu_p = 0.25$ for the pile; (4) pile–soil mass density contrast ($\rho_{p/}\rho_s$) = 2; and (5) material (hysteretic) damping ratio $\beta_s = 0.05$ for soil and $\beta_p = 0.01$ for pile. Except for the simulations of the dynamic experiments, a pile modulus of elasticity (E_p) of 3×10^7 kPa (indicative of concrete) was used along with a pile diameter (d) of 1 m in the FE analyses. The modulus of elasticity of soil was consequently estimated from the pile–soil stiffness contrast (E_p/E_s). The presented elastic solutions are expressed in dimensionless forms and can be used for any type of pile using an equivalent axial elastic modulus. Over 500 FE analyses were carried out in total [45].

4. Model Validation and Parameter Analyses

4.1. Static Loading Conditions

The K-PAX FE model was thoroughly validated against established results from the literature. For static conditions, infinite elements were employed at the boundaries of the mesh to replicate the half-space.

Static pile-head stiffnesses were computed for a pile embedded in three different soil profiles with varying pile–soil stiffness contrast (E_p/E_{sL}) and compared to published results by El-Sharnouby & Novak [53] in Figure 4. We note that the normalized pile stiffness appears to increase as soil stiffness (E_{sL}) decreases, which is counterintuitive. Nevertheless, this trend is anticipated, because E_{sL} is also used to normalize the pile-head stiffness K_z. The actual value of K_z decreases with a decrease in E_{sL}. A homogeneous profile naturally leads to stiffer conditions at the pile head, for it encompasses stiffer soil close to the surface than the vertically inhomogeneous profiles of equal Young's modulus at the pile tip ($E_s = E_{sL}$). The agreement between the two solutions is satisfactory. Additional comparisons between results from the present study and the rigorous numerical solution of El-Marsafawi et al. [54] indicate maximum deviations in stiffness of less than 3% [45].

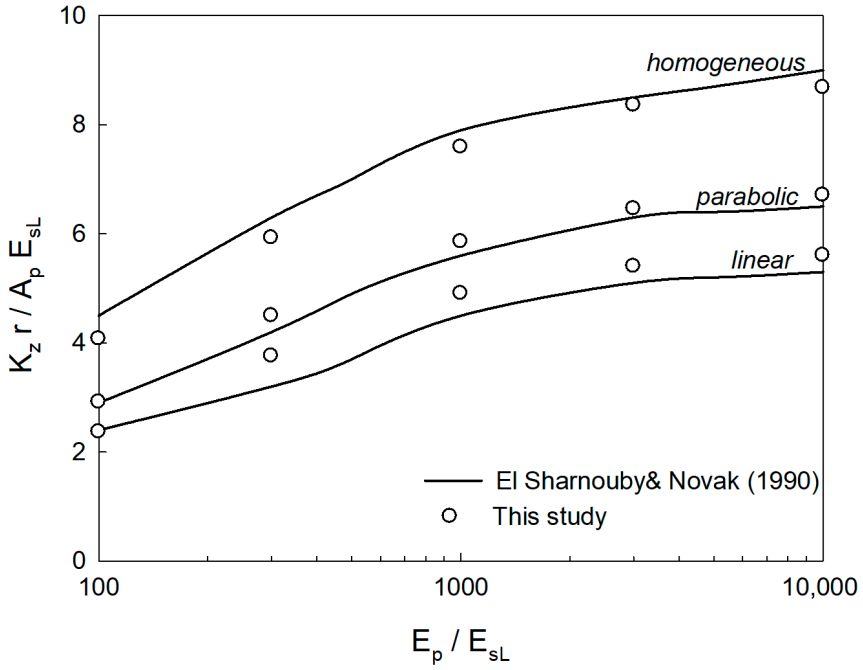


Figure 4. Normalized vertical static stiffness of a floating pile in various soil profiles. Comparison of the proposed solution with results from the literature; ν_s = 0.5, L/d = 25. The parabolic profile considered by El-Sharnouby & Novak [53] is defined by Equation (3) with the ratio z/L raised to the power of ½.

The effect of radial soil inhomogeneity under static loading was next investigated for the above E_p/E_{sL} values used in Figure 4. Tables 1 and 2 show reduction in pile stiffness with increasing levels of radial inhomogeneity (higher A values). Evidently, for high levels of radial inhomogeneity (A = 0.8), pile-head stiffness may drop by as much as 30 percent. The specific trend becomes stronger for softer soils (higher E_p/E_s). This observation is in accordance with earlier findings that using far-field soil moduli (i.e., completely ignoring installation or loading effects) might lead to underestimation of pile settlements [55].

Table 1. Comparison of normalized static stiffness of floating piles, embedded in Homogeneous and a Radial soil for different levels of radial inhomogeneity (A).

L/d	$E_p/E_{s,\infty}$	A = 0	A = 0.1		A = 0.5		A = 0.8	
		$K_z\, d/E_s$	$K_z\, d/E_{s\infty}$	(%)	$K_z\, d/E_{s\infty}$	(%)	$K_z\, d/E_{s\infty}$	(%)
20	100	6.26	5.99	−4.3	5.24	−16.3	4.50	−28.1
	300	8.69	8.29	−4.6	7.13	−18.0	5.99	−31.1
	1000	10.54	9.99	−5.2	8.42	−20.1	6.93	−34.3
40	100	6.47	6.21	−4.0	5.49	−15.1	4.82	−25.5
	300	10.02	9.64	−3.8	8.18	−18.4	7.58	−24.4
	1000	14.52	13.91	−4.2	12.11	−16.6	10.26	−29.3
60	100	6.48	6.22	−4.0	5.50	−15.1	4.83	−25.5
	300	10.26	9.90	−3.5	8.87	−13.5	7.85	−23.5
	1000	16.07	15.49	−3.6	13.77	−14.3	11.97	−25.5

Table 2. Comparison of normalized, static stiffness of floating piles, embedded in Linear and Linear-Radial soil for different levels of radial inhomogeneity (A).

L/d	$E_p/E_{sL,\infty}$	A = 0	A = 0.1		A = 0.5		A = 0.8	
		$K_z\ d/E_{sL}$	$K_z\ d/E_{sL\infty}$	(%)	$K_z\ d/E_{sL\infty}$	(%)	$K_z\ d/E_{sL\infty}$	(%)
20	100	3.81	3.66	−3.9	3.24	−15.0	2.81	−26.2
	300	5.60	5.34	−4.6	4.57	−18.4	3.84	−31.4
	1000	6.86	6.48	−5.5	5.41	−21.1	4.44	−35.3
40	50	2.18	2.11	−3.2	1.92	−11.9	1.74	−20.2
	150	4.17	4.04	−3.1	3.66	−12.2	3.27	−21.6
	500	7.37	7.08	−3.9	6.22	−15.6	5.35	−27.4

A nonlinear regression analysis of the above data using the Levenberg–Marquardt method [56] provided the following expressions for static pile stiffness that can be easily implemented on a spreadsheet:

For vertically homogeneous profiles (i.e., Homogeneous and Radial),

$$K_z = 1.8E_{s\infty}d\left(\frac{L}{d}\right)^{0.65}\left(1-0.4A^{0.73}\right)\left(\frac{E_p}{E_{s\infty}}\right)^{-0.5(1-0.17A^{0.63})\left(\frac{L}{d}\right)^{0.7}\left(\frac{E_p}{E_{s\infty}}\right)^{-0.7}} \quad (6)$$

For vertically inhomogeneous profiles (i.e., Linear, Linear-Radial),

$$K_z = 1.8E_{sL\infty}d\left(\frac{L}{d}\right)^{0.55}\left(1-0.34A^{1.2}\right)\left(\frac{E_p}{E_{sL\infty}}\right)^{-0.5\left(\frac{L}{d}\right)^{0.6}\left(\frac{E_p}{E_{sL\infty}}\right)^{-0.6}} \quad (7)$$

The correlation coefficient R^2 of the first equation against the source data is 0.985, and of the second, 0.984.

From Equation (7), the effect of radial soil inhomogeneity on pile stiffness is determined as a reduction factor of $(1 - 0.34\ A^{1.2})$. For A = 0.8, this factor is 0.74 (a 26% reduction), which is comparable with the results of Table 2.

In the special case of radially homogeneous soil (A = 0), the above equations reduce to

$$K_z = 1.8\ E_s\ d\left(\frac{L}{d}\right)^{0.65}\left(\frac{E_p}{E_s}\right)^{-0.5\left(\frac{L}{d}\right)^{0.7}\left(\frac{E_p}{E_s}\right)^{-0.7}} \quad (8)$$

and

$$K_z = 1.8\ E_{sL}\ d\left(\frac{L}{d}\right)^{0.55}\left(\frac{E_p}{E_{sL}}\right)^{-0.5\left(\frac{L}{d}\right)^{0.6}\left(\frac{E_p}{E_{sL}}\right)^{-0.6}} \quad (9)$$

for Homogeneous and Linear soil, respectively. Equation (8) provides a simple equation that can be used to obtain first-order estimates of an equivalent homogeneous soil modulus using static pile load test settlement results. The above formulas yield predictions that are comparable to those obtained from available expressions in the literature [30].

4.2. Dynamic Loading Conditions

For harmonic steady-state conditions, pile-head displacement is typically determined as a complex quantity describing both amplitude and phase difference between excitation and response due to hysteretic action and wave propagation in the medium. Accordingly, dynamic pile-head stiffness is represented by a complex dynamic "impedance", K_z, com-

posed of a real part, representing stiffness, and an imaginary part, representing damping. This function can be cast in the following equivalent forms:

$$K_z = K_z(\omega) + i\,\omega\,C_z = K_z(\omega)\,(1 + 2\,i\,\beta_z) \tag{10}$$

where $K_z(\omega)$ = real part and $(\omega\,C_z)$ = imaginary part of the dynamic impedance, ω = cyclic excitation frequency, C_z = dashpot coefficient, and $\beta_z = \omega\,C_z/(2\,K_z)$ = dimensionless damping coefficient incorporating material and radiation damping. The last coefficient is particularly useful for assessing the damping properties of the pile–soil system, for it is analogous to the critical damping ratio in a viscously damped simple oscillator [29].

In Figure 5, the real and imaginary parts of K_z are plotted against dimensionless excitation frequency for a pile in homogeneous soil. The predictions of the finite-element results follow closely those of El-Marsafawi et al. [54]. Additional verifications for piles in Linear soil profiles and in profiles with two soil strata are provided in Syngros [45]. It is evident from these data that the real part of dynamic impedance tends to increase with frequency and that this increase is stronger for softer soils. The imaginary part increases almost linearly with frequency beyond $a_0 = 0.2$, which suggests an approximately frequency-independent dashpot coefficient C_z.

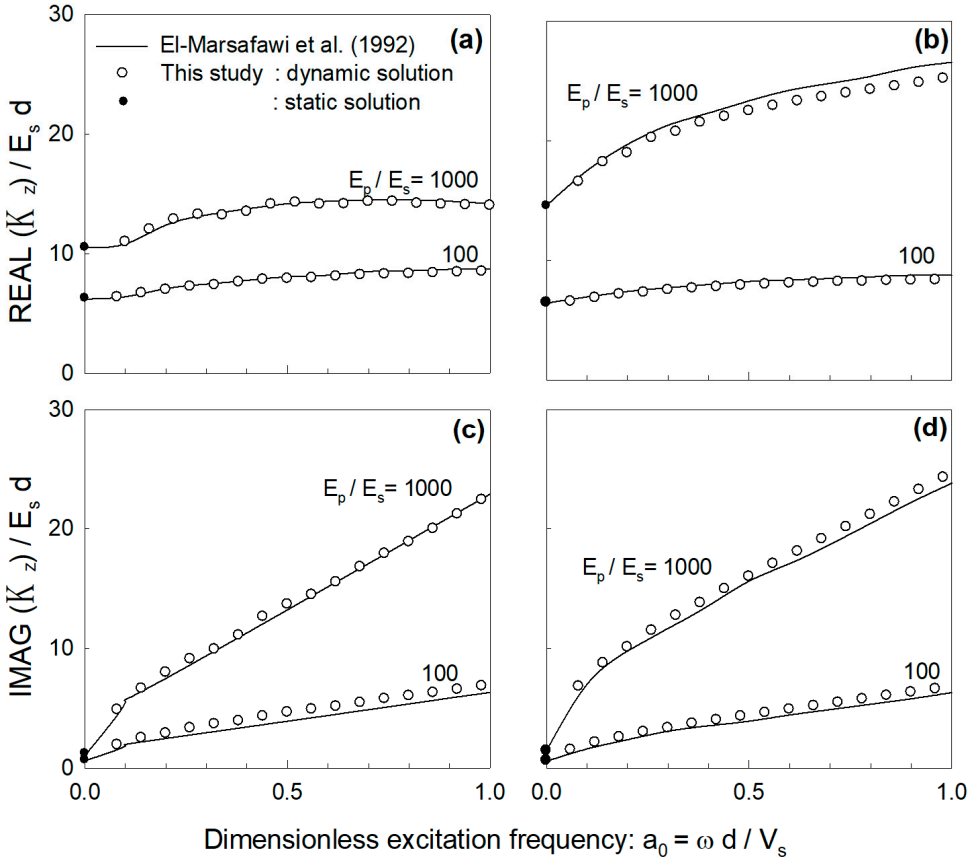


Figure 5. Normalized axial dynamic stiffness of a floating pile in homogeneous soil for two different stiffness pile–soil contrasts (El-Marsafawi et al. [54]); Cases (**a**,**c**): $L/d = 20$; Cases (**b**,**d**): $L/d = 40$.

Dynamic pile impedance is further explored in Figure 6, where the real and imaginary parts of K_z are plotted against dimensionless frequency for soil profiles with different degrees of radial inhomogeneity (A). All profiles have the same elastic properties in the far-field ($r \longrightarrow \infty$) and underneath the pile tip ($z > L$) (i.e., $E_s = E_{sL} = E_{s\infty} = E_{sL\infty}$). It can be observed that radial inhomogeneity reduces dynamic stiffness at all frequencies and alters the slope of dynamic stiffness curves. Note that for strong vertical and radial inhomogeneity

(i.e., Linear-Radial soil with A = 0.8) and high excitation frequencies (a_0 > 0.9), the real part of dynamic stiffness may become negative. This behavior is admissible for dynamic loads and should not come as a surprise (e.g., it exists in the simple oscillator), as it merely suggests a phase difference between load and displacement at the pile head greater than 90 degrees. It should be noticed that at very low frequencies, the numerical curves exhibited some undulations which could be attributed to numerical instabilities associated with the cut-off frequency of the layer. Instead, the static result is shown where the static and dynamic solutions should converge.

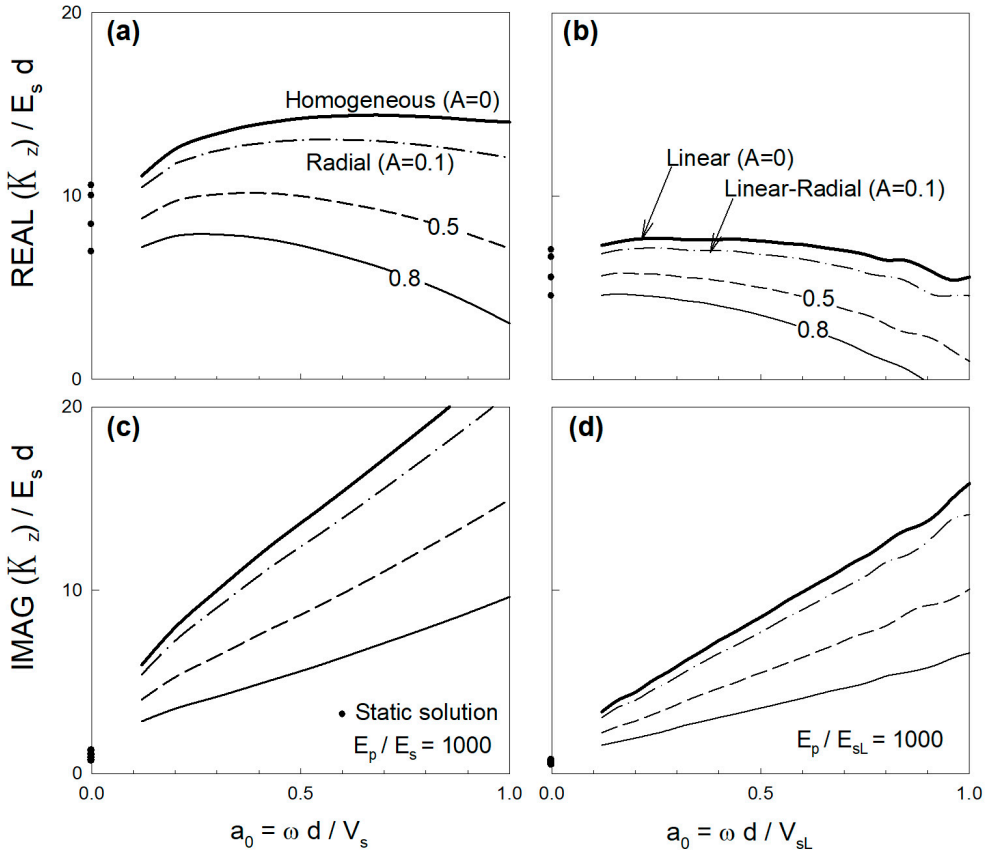


Figure 6. Normalized dynamic vertical pile-head stiffness of a floating pile in various soil profiles with the same elastic soil properties at the far-field (**a**,**c**) and below the pile (**b**,**d**) tip; L/d = 20.

4.3. Effect of Soil Inhomogeneity on Pile Damping—Stiffness-Equivalent Soil Profiles

It is well known that energy dissipation in an unbounded medium arises from two distinct sources: (1) material damping, where energy is consumed through hysteretic action (notably friction), and (2) radiation damping, where energy is emitted to infinity in the form of body and surface waves propagating in the unbounded medium, even if the material is perfectly elastic.

In this light, the damping ratio in Equation (10) can be decomposed as

$$\beta_z = \beta_z(\omega) = Im(K_z)/[2\ Re(K_z)] = \beta_z^{radiation}(\omega) + \beta_z^{material} \quad (11)$$

where $\beta_z^{radiation}$ pertains to wave radiation and $\beta_z^{material}$ to hysteretic action. Note that the former type of damping is inherently frequency dependent (hence the notation in Equation (11)), whereas the latter is essentially frequency independent for the majority of geomaterials.

The way soil inhomogeneity affects radiation damping is not easy to assess. Intuition suggests that in an inhomogeneous medium, the waves emitted from an oscillating pile

tend to bend and become gradually refracted back to the source; thereby, less energy is radiated to infinity as compared to a perfectly homogeneous soil. This effect tends to reduce the imaginary part of K_z with increasing inhomogeneity factor A in Equation (1) (also seen in Figure 6). On the other hand, increasing soil inhomogeneity will also reduce—by a different amount—the real part of K_z and alter the dimensionless frequency factor a_0 (=$\omega\, d/V_s$). Therefore, both the numerator and denominator in Equation (11) will decrease and dimensionless frequencies will shift, complicating comparisons of pile response at different inhomogeneity levels. It is noted in passing that the negative real part of K_z merely suggests a phase difference between excitation and response greater than 90° (between 90° and 270°). In practice, an engineer can divide the amplitude of the force by the amplitude of the impedance to determine the amplitude of pile-head displacement, disregarding phase.

To elucidate this, β_z is plotted against dimensionless frequency a_0 for three pile–soil stiffnesses contrasts in Homogeneous and Linear soil (Figure 7a,b). To ensure that same ω's correspond to same a_0's, the abscissas are normalized by a common shear wave velocity based on the curve for E_p/E_s = 1000. An increase in damping with increasing E_p/E_s (softer soils) is apparent in all plots. Evidently, no clear difference in damping between homogeneous (Figure 7a) and inhomogeneous (Figure 7b) profiles is observed, especially for the two lower curves (E_p/E_s = 100 and 300).

Radially inhomogeneous profiles are examined in Figure 7c,d for Radial and Linear-Radial stiffness variations, respectively. All profiles have a common pile stiffness E_p and far-field soil modulus $E_{sL\infty} = E_p/1000$. To ensure a common frequency axis, a_0 is normalized by a single shear wave velocity $V_{sL\infty}$ pertaining to the far-field modulus $E_{sL\infty}$. It appears that the stronger the inhomogeneity (i.e., the higher the value of A or the softer the soil profile), the lower the damping ratio in the frequency range $a_0 < 0.7$. The trend is analogous to the one observed in Figure 7a,b, yet reverses for $a_0 > 0.7$. No clear effect of soil inhomogeneity on radiation damping can be gleaned from these graphs.

The reasons for the above ambiguities should be sought in the different pile stiffnesses involved in the various curves. Strictly speaking, damping ratios in two viscoelastic systems are directly comparable only if the systems have matching stiffnesses. In the case of two axially, harmonically loaded piles, this can be achieved if the far-field (reference) soil moduli are selected in such a way that the resulting stiffnesses at the head of the piles are equal. To satisfy the above condition, a trial-and-error method could be used to find "equivalent" soil moduli, or Equations (6) and (7) could be used to obtain the following simplified expressions from relating soil moduli in the various profiles:

$$\left(\frac{E_p}{E_{sL}}\right) = 4.1\left(\frac{L}{d}\right)^{-0.85}\left(\frac{E_p}{E_s}\right)^{0.9\left(\frac{L}{d}\right)^{0.065}} \quad \text{(Linear } E_{sL} \text{ from Hom. } E_s\text{)} \tag{12}$$

$$\left(\frac{E_p}{E_{s\infty}}\right) = (1 - 0.45A)\left(\frac{E_p}{E_s}\right) \quad \text{(Radial } E_{s\infty} \text{ from Hom. } E_s\text{)} \tag{13}$$

$$\left(\frac{E_p}{E_{sL\infty}}\right) = (1 - 0.47A)\left(\frac{E_p}{E_{sL}}\right) \quad \text{(Linear Radial } E_{sL\infty} \text{ from Linear } E_{sL}\text{)} \tag{14}$$

Stiffness pairs obtained from the above relations produce soil profiles of equal stiffness to be referred to in this work as "stiffness equivalent". Note that statically equivalent soil profiles can also be obtained for inhomogeneous profiles of the *same* type. For instance, from Equation (13), it is a simple matter to show that two Radial soil profiles are stiffness-equivalent if:

$$\left(\frac{E_p}{E_{sL\infty}}\right)_1 = \left(\frac{1 - 0.45A_1}{1 - 0.45A_2}\right)\left(\frac{E_p}{E_{sL\infty}}\right)_2 \tag{15}$$

where $(E_p/E_{s\infty})_1$ and $(E_p/E_{s\infty})_2$ are the characteristic stiffness contrasts and A_1 and A_2 the corresponding inhomogeneity factors. Similar relations can be obtained for the other profiles.

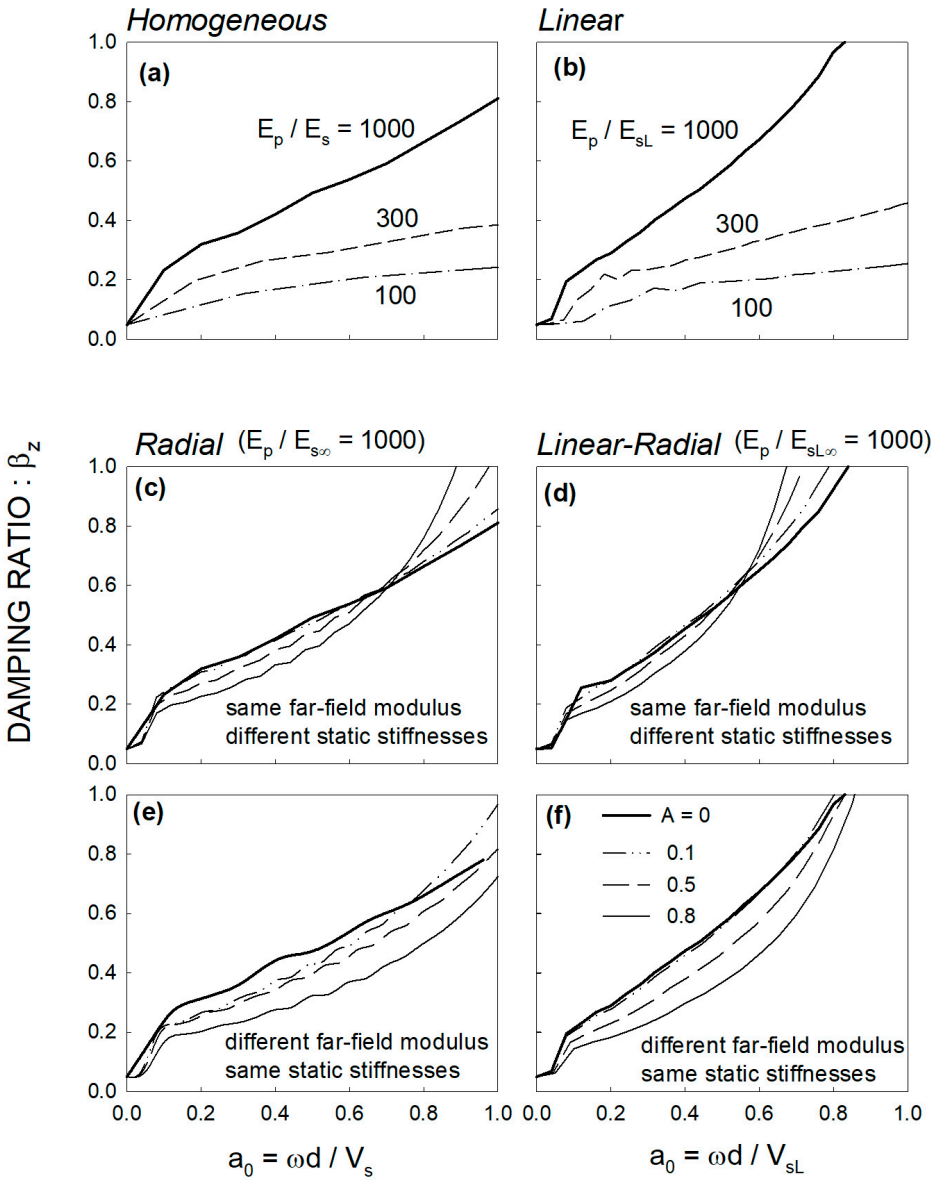


Figure 7. Equivalent damping ratio at the pile head for various soil profiles (**a**–**f**). In all plots, ω is normalized with V_s. corresponding to $E_s = E_p/1000$. In graph (**e**), $E_p/E_{s\infty}$ = 1000, 980, 810 and 650 in the four curves, respectively, according to Equation (15). In graph (**f**), corresponding values are 1000, 970, 790, 640.

Results for stiffness-equivalent soil profiles are presented in Figure 7e,f, referring to Radial and Linear-Radial modulus variations. From these plots, it appears that inhomogeneous profiles consistently radiate less energy than stiffness-equivalent profiles of weaker inhomogeneity over a wide range of frequencies. Considering this observation, the effect of soil inhomogeneity on radiation damping becomes apparent only when the β_z versus a_0 plots are adjusted both for frequency and soil stiffness.

Following the above adjustments, the effect of soil inhomogeneity on radiation damping becomes even more obvious in Figure 8, where four stiffness-equivalent soil profiles are examined. To ensure a common frequency axis, a_0 is normalized with the shear wave velocity for the Homogeneous profile. For $a_0 = 0.2$, radiation damping for the Homogeneous profile is 26% as opposed to a mere 11% for the Linear-Radial profile. For higher frequencies, the differences can be even greater. This is an interesting behavior given that actual soil profiles

are rarely homogeneous. It suggests that if one ignores soil inhomogeneity, the estimated damping may be unreasonably high. In addition, if one adopts a low modulus of elasticity for the soil (a typically conservative design assumption for static loading), the estimated radiation damping may turn out unreasonably high (see Figure 7a,b)—an unconservative behavior for dynamic loading. Evidently, modeling assumptions that yield conservative designs for static loads may be unconservative for dynamic loads, and vice versa.

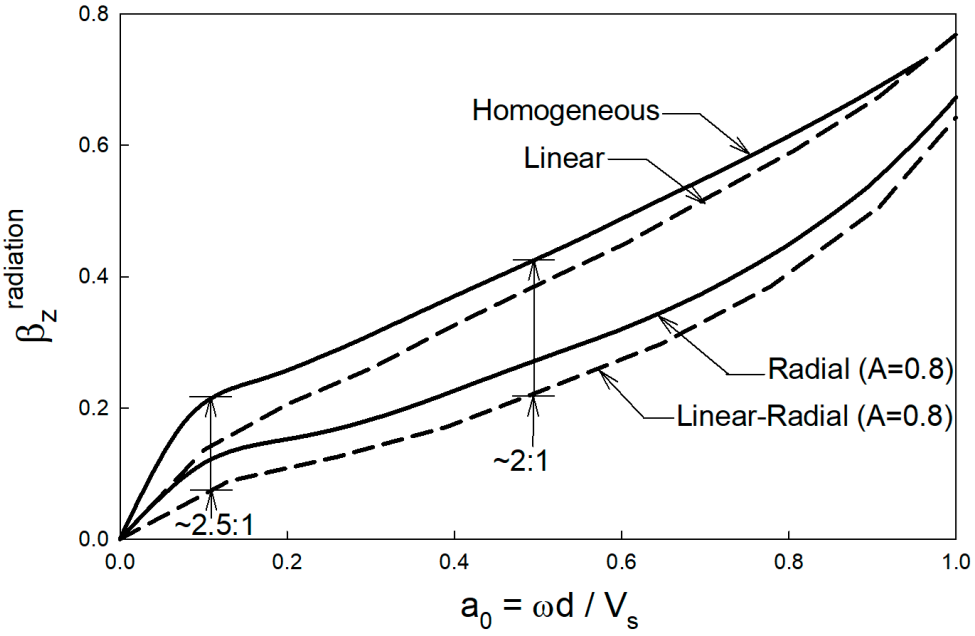


Figure 8. Radiation damping at the pile head for stiffness-equivalent soil profiles. Note the decrease in radiation damping with increasing soil inhomogeneity; L/d = 20, E_p/E_s = 1000. Dimensionless frequency is obtained for vs. corresponding to the Homogeneous profile.

In the frequency range $0.1 < a_0 < 0.5$, the following approximate relation can be obtained for radiation damping in homogeneous soil and in soil with double inhomogeneity:

$$\left(\beta_z^{radiation}\right)_{\substack{soil\ with\ double \\ inhomogeneity}} \approx 0.4 \div 0.5 \left(\beta_z^{radiation}\right)_{homogeneous\ soil} \quad (16)$$

which can be used as a rule of thumb for assessing radiation damping in practical applications. This relation was found to provide reasonable predictions for a large set of numerical simulations encompassing different E_p/E_s ratios in both axial and flexural oscillations [45]. Note that the above behavior results from purely viscoelastic analysis and does not explicitly encompass strain effects. Comparisons against field tests to be presented in the remainder of this article suggest that Equation (16) provides good estimates of radiation damping for relatively small pile-head loads. For strong nonlinear response, soil damping is expected to be even lower than 40 to 50% of that for the equivalent homogeneous soil.

4.4. Dynamic Winkler Spring Stiffness

The Winkler impedance k_z along the pile is defined in a similar manner as in Equation (10):

$$k_z = p(z)/w(z) = Re(k_z) + i\ Im(k_z) = k_z + i\ \omega\ c_z = k_z\ (1 + 2\ i\ \beta_z) \quad (17)$$

where $p(z)$ = soil reaction per unit pile length at depth z; $w(z)$ = pile displacement at the same depth, k_z, c_z = moduli of Winkler springs and dashpots, and β_z = damping ratio incorporating both material and radiation damping. Note that for a complete representa-

tion of soil reaction, a frequency-dependent spring and dashpot at the pile-tip should be included to account for stiffness and damping of the soil material under the pile. This type of reaction is not discussed here.

Figure 9 shows four soil profiles having the same far-field properties, (i.e., $E_s = E_{sL} = E_{s\infty} = E_{sL\infty}$). Normalized real and imaginary parts of dynamic impedance at each depth are plotted for five dimensionless frequencies, a_0 (an a_0 value of zero corresponds to static loading). The following main trends are observed: (1) k_z, c_z exhibit a distinct jump at both the pile head and tip (an edge layer phenomenon attributed to the boundary conditions, [57]), (2) frequency dependence of both parameters is suppressed with increasing soil inhomogeneity, and (3) the empirical expressions by Roesset [58] and Gazetas et al. [59] compare well with the numerical results for homogeneous soil, but not as successfully for inhomogeneous soil.

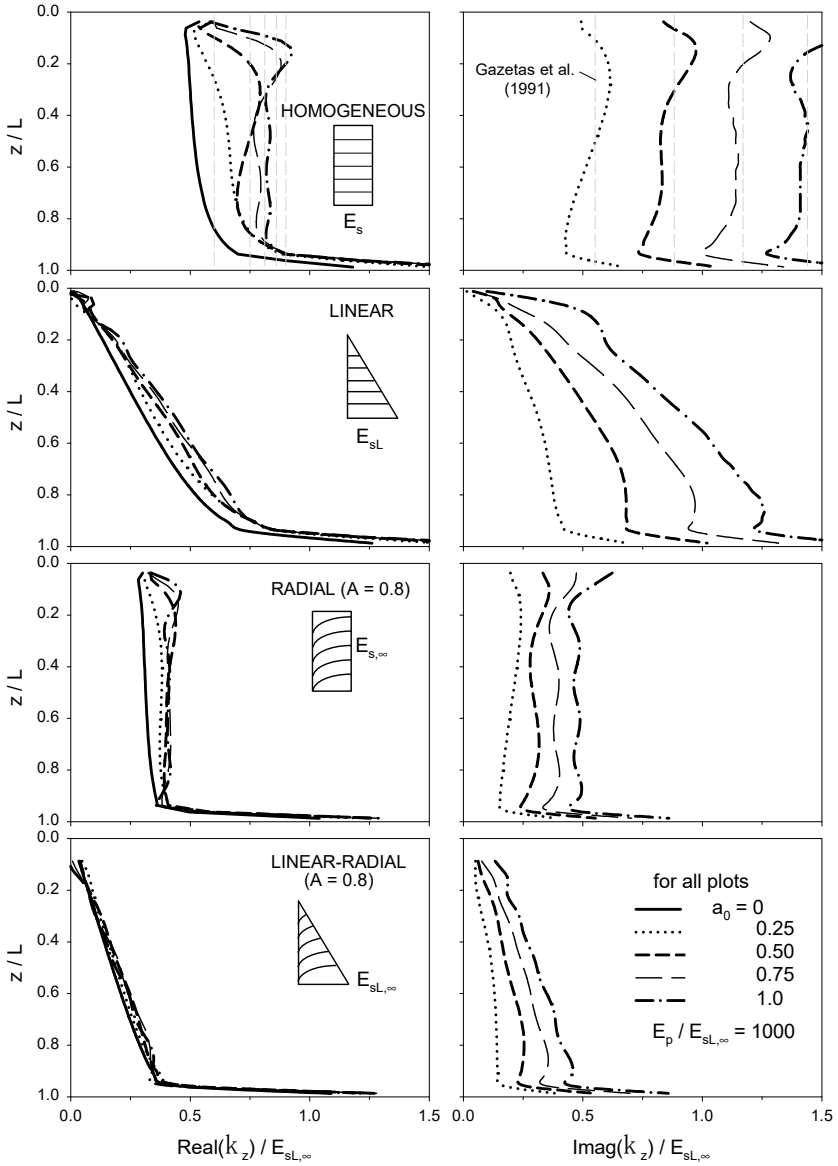


Figure 9. Real and imaginary part of distributed Winkler impedance along a floating pile in different soil properties for selected frequencies; $L/d = 20$. Note that the imaginary part is essentially zero at $a_0 = 0$. Note that if one combines vertical and radial inhomogeneities, it can produce different target stiffnesses. However, if vertical inhomogeneity is treated as an intrinsic (pre-existing) soil property, the equivalence between a radially homogeneous and inhomogeneous soil profile under the same vertical stiffness variation is unique [59].

Additional insight is provided in Figure 10, where normalized displacements, soil reactions and Winkler moduli are presented for four stiffness-equivalent soil profiles at two different frequencies. The following trends are observed: (1) pile displacements for radially homogeneous soil profiles (i.e., Homogeneous and Linear) attenuate faster with depth than for radially inhomogeneous profiles (i.e., Radial and Linear-Radial), with the differences being more pronounced at higher frequencies. On the contrary, (2) soil reactions for vertically homogeneous and inhomogeneous profiles are similar for all frequencies examined. (3) Normalized Winkler moduli ($\delta = k_z/E_s$) follow the same trends as pile displacement and are similar for radially homogeneous and inhomogeneous profiles. This implies that, contrary to soil reaction, Winkler modulus is controlled by the soil properties (E_s) adjacent to the pile.

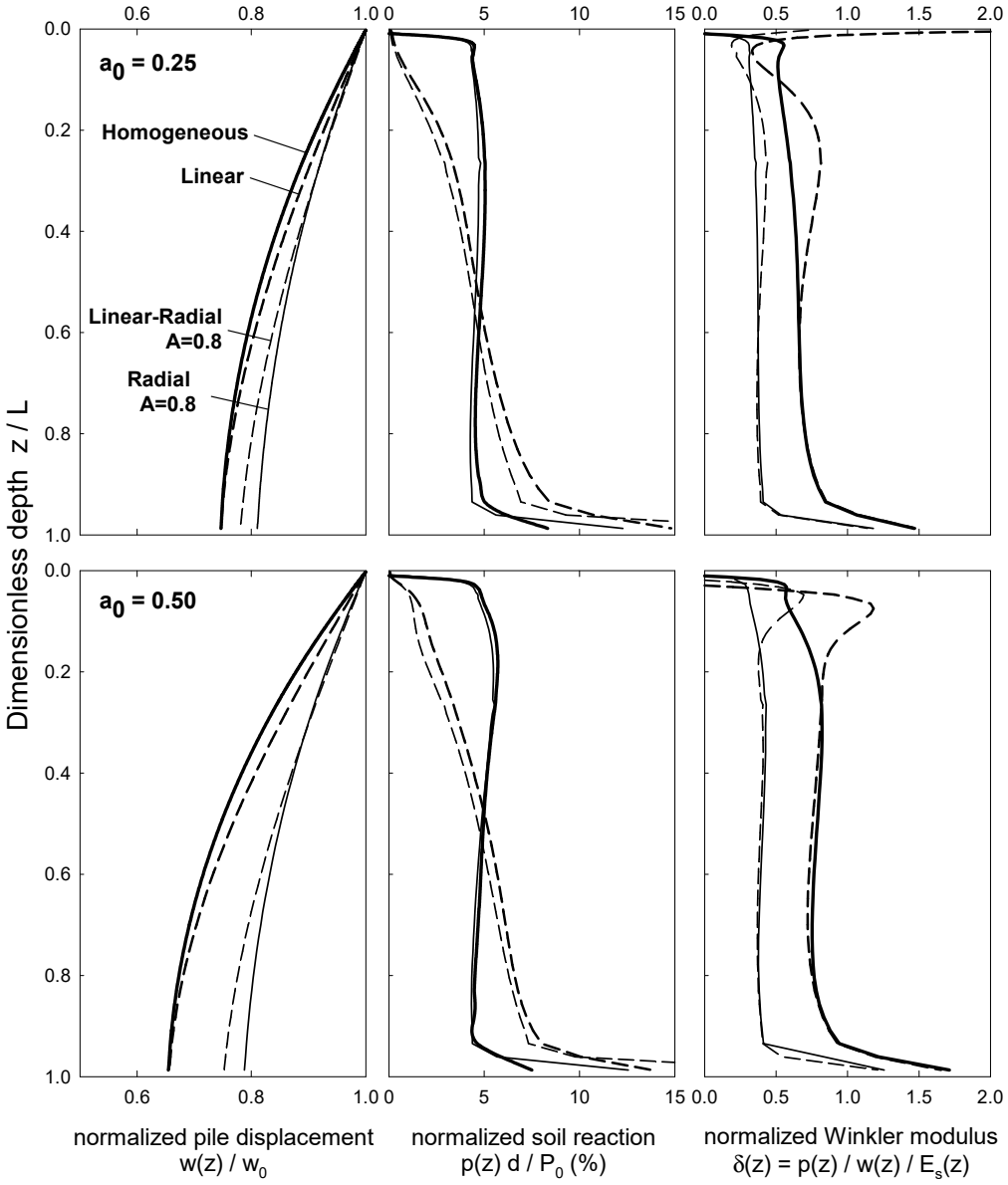


Figure 10. Real parts of pile stiffness, displacement, soil reaction, and Winkler modulus for a floating pile in four stiffness-equivalent soil profiles at two excitation frequencies; L/d = 20, E_p/E_s is 1000, 630, 650, and 380 for the Homogeneous, Linear, Radial and Linear-Radial profiles, respectively.

Distributed damping ratios β_z are plotted in Figure 11 along with distributed stiffnesses k_z for the same soil profiles. As a general trend, β_z decreases with increasing radial

inhomogeneity—in accordance with the previous discussions. No clear trends are visible for the variation of β_z with depth, especially in homogeneous soil.

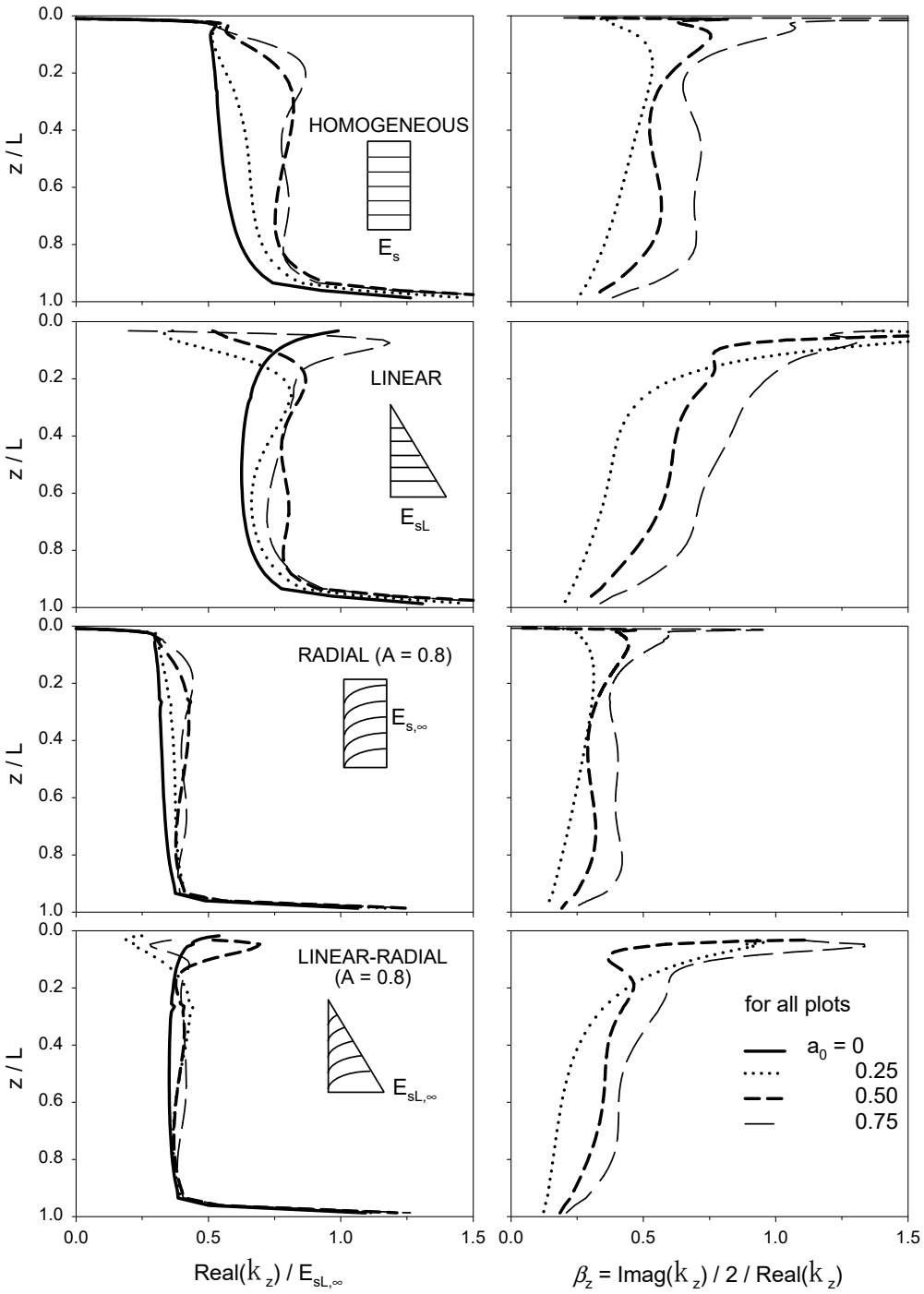


Figure 11. Real and imaginary part of distributed Winkler impedances in four stiffness-equivalent soil profiles; L/d = 20. Pile–soil stiffness contrasts are as in Figure 10.

5. Comparisons with Experimental Results

The numerical analysis described in the previous sections was employed to simulate measurements from dynamic experiments on single piles and pile groups, as reported by El-Marsafawi et al. [54] and Blaney et al. [60] (see also references [61–64]). Because of space limitations, only a brief description of the soil profiles and experimental procedures

is provided below. For a more complete presentation, the reader is referred to the original publications and to Syngros [45].

5.1. Dynamic Experiments by El-Marsafawi et al. [54]

El-Marsafawi et al. [54] investigated the response of steel model piles by attaching a rigid mass (cap) at the pile head and exciting the system harmonically using a shaker equipped with rotating masses. Pile and soil properties are shown in Figure 12a. The measured displacement amplitude was given by El-Marsafawi et al. [54] in the dimensionless form $D_z = (m_{cap}\, u_z / m_e\, e)$, where the quantity $(m_e\, e)$ in the denominator stands for an "excitation intensity", with m_e being the exciting mass and e the eccentricity. It is noted that, in the realm of elastodynamic theory, the above normalized amplitude is independent of excitation intensity. Measured and computed responses are compared in Figure 13. Evidently, the behavior of the actual system is nonlinear, as the measured resonant frequencies and response amplitudes depend on the amplitude of the applied load.

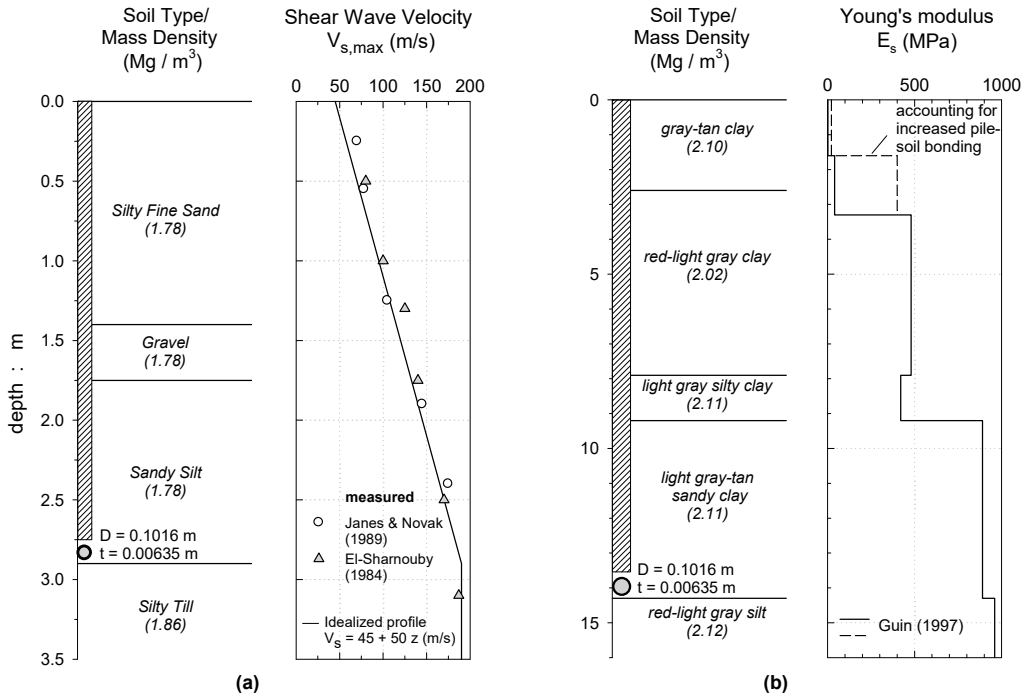


Figure 12. Soil properties at University of Western Ontario test site according to Janes & Novak [65] and El-Sharnouby [64] (**a**) and University of Houston test site (**b**) [63]. Modified after El-Marsafawi et al. [54] and Blaney et al. [60], respectively.

The information presented in Figure 13 indicates that the conventional assumption of radially homogeneous soil ($A = 0$) overestimates pile–soil resonant frequency and underestimates the displacement response at the pile head. This suggests an overly stiff, overdamped soil compared to the measurements. On the other hand, considering an equivalent radial inhomogeneity ($A = 0.8$), both resonant frequency and response amplitude are closer to the observed. Even for this case, however, the predicted response at resonance is lower than the measured one by a factor of 2 or so. This suggests that damping in the analyses is twice as high as the actual damping in the system, despite the small values of material damping considered ($\beta_p = 1\%$, $\beta_s = 3.5\%$). A theoretical prediction obtained assuming zero radiation damping is also shown. It is obvious that such an assumption is highly conservative, as it over-predicts displacement response by a factor of 2.5. The above findings elucidate the importance of radiation damping in controlling pile response and, thereby, the necessity to

incorporate this type of damping in the analysis and how challenging it is to estimate the pile dynamic response, particularly near resonance.

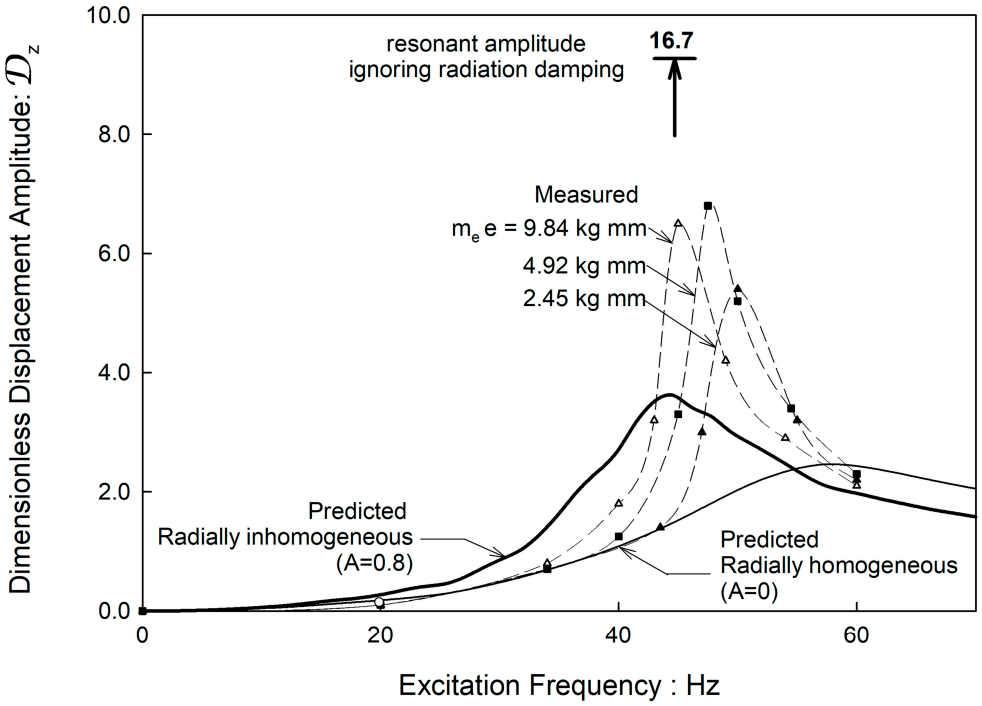


Figure 13. Comparison of measured and predicted response of a single steel model pipe pile (El-Marsafawi et al. [54]). Note the overestimation of pile–head resonant frequency and damping assuming radially homogeneous soil (A = 0) and the improved prediction considering radial soil inhomogeneity (A = 0.8).

5.2. Dynamic Experiments by Blaney et al. [60]

Blaney et al. [60] investigated the response of full-scale steel pipe piles. Test properties are shown in Figure 12b. Figure 14 shows predicted and measured response of a single pile. Evidently, incorporating radial inhomogeneity (A = 0.8) yields very good predictions of pile response. Like before, assuming zero radiation damping significantly over-predicts, by a factor of 2.5, response at resonance.

A result for pile group response based on Blaney's [60] data is provided in Figure 15 for a 3 × 3 square pile configuration. Although pile group effects are not the focus of this paper (recall that even with only two piles, the pile group problem is not axisymmetric and, thereby, modeling involving wave propagation in three dimensions is needed), they are examined here to elucidate the applicability of the analysis at hand to more general situations. Details on theoretical aspects of these simulations, where the solutions of a single pile are used in conjunction with the superposition method to account for pile-to-pile interaction, are given in Kaynia & Kausel [21], Syngros [45] and in Mylonakis & Gazetas [66].

The response curves are much flatter relative to those for a single pile (Figure 14), without exhibiting a distinct resonant peak. The simulations are clearly not as good as those for the single pile on the same site. Nevertheless, considering radial soil inhomogeneity (A = 0.8) yields improved predictions relative to the classical assumption of homogeneous soil. This trend was found to be consistent for different experimental setups and oscillation modes, as discussed in Syngros [45]. We theorize that discrepancies between simulations and field measurements (notably in Figure 13) have to do with phenomena not captured in the theoretical solutions, such as soil material nonlinearity, imperfect pile–soil bonding, or even variability in field measurements of soil parameters.

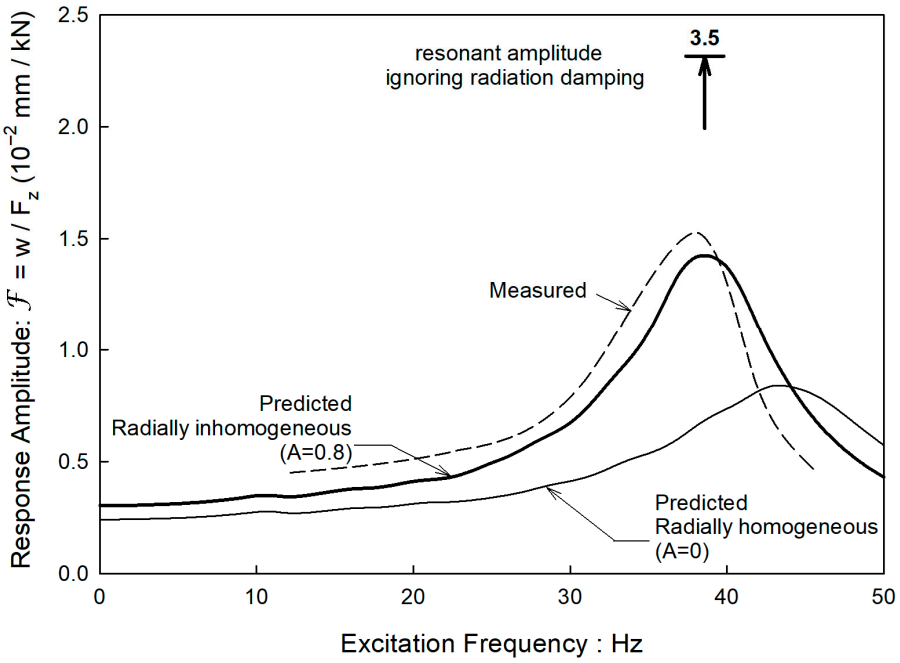


Figure 14. Comparison of measured and predicted response of a full-scale single steel pipe (Blaney et al. [60]). Note the overestimation of resonant frequency and damping assuming radially homogeneous soil (A = 0) and the improved prediction considering radial inhomogeneity (A = 0.8).

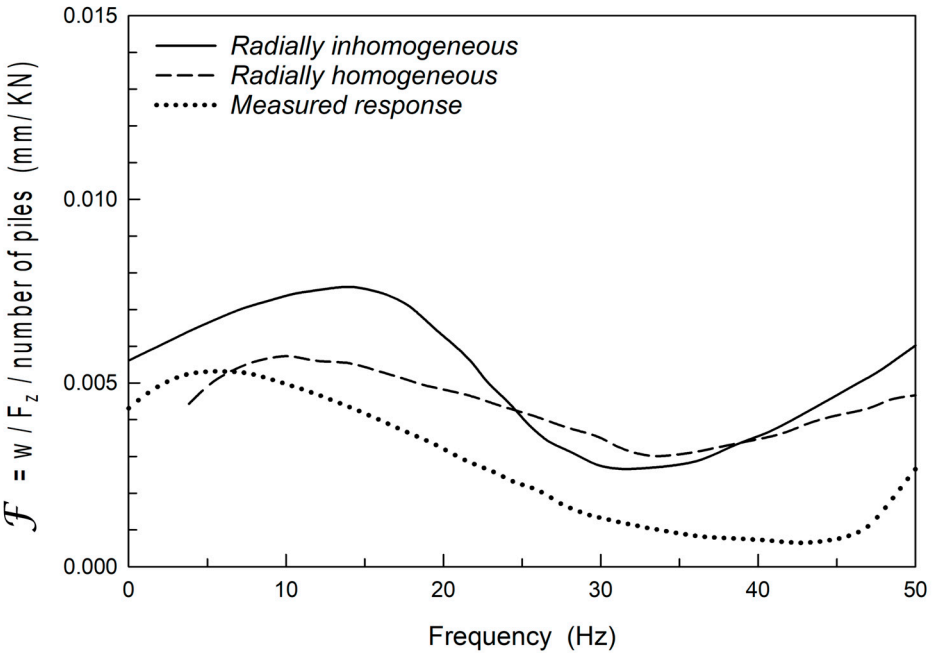


Figure 15. Comparison of the measured and computed vertical response of a steel pile group in the University of Houston site (Blaney et al. [60]). Note the improved predictions considering radial inhomogeneity.

6. Discussion

We note that the formulation assumes linear viscoelastic soil behavior throughout; accordingly, the results are more applicable for low-strain amplitudes, where the load and displacement amplitudes are kept low. This formulation allows us to peek into possible causes (such as double inhomogeneity) of radiation damping that are appreciably lower than what a homogeneous soil or rock profile would generate. As load amplitudes

and strains become higher, radiation damping becomes even harder to estimate, with material/hysteretic damping starting to increase, and the pile stiffness starting to decrease. That is why it is important in design to perform sensitivity studies and allow for variability in assumed parameters but also in the underlying assumptions such as effects of soil/rock nonlinearity. We note that in such sensitivity studies, an estimated material damping ratio that arises from nonlinear effects in the soil can be incorporated in Equation (10).

Depending on the type of pile and installation technique, the Young's modulus of the adjacent soil or rock may be increased (for example, driven, displacement type piles in sand) or decreased (for example, drilled shafts in rock using bentonite slurry, or overcutting soils during installation of micro-piles in sands). The present study sheds some light in general on the effects of inhomogeneity that can be used in sensitivity studies during the design of piles. Such effects appear to be more prevalent for a_0 greater than about 0.2 and for Ep/Es greater than about 500.

7. Conclusions

The main conclusions of the study are as follows:

(1) Ignoring radial soil inhomogeneity (reflecting installation and loading effects in the soil surrounding the pile) may lead to underestimation of static pile settlement by as much as 30%. Accordingly, use of far-field ("undisturbed") soil moduli may result in reduced pile settlement estimates.

(2) Radiation damping drops significantly with increasing soil inhomogeneity. In a homogeneous half-space, it can be more than twice that in a soil with double inhomogeneity (Figure 8). Therefore, damping coefficients recommended in foundation engineering manuals based on assumptions of homogeneous half-space conditions should be employed with caution. As a rule of thumb, a reduction in radiation damping by a factor of 2 to 2.5 is recommended for relatively small pile-head loads (Equation (16)).

(3) Modeling an inhomogeneous soil profile as an equivalent homogeneous medium with reduced modulus of elasticity, although routinely used for pile settlement analysis under static loads, may severely underestimate pile-head displacements under dynamic conditions and poorly predict the resonant frequency. This is because homogeneity in the soil tends to increase radiation damping and alter the dynamic stiffness of the pile–soil system.

(4) The assumption of zero radiation damping tends to severely overestimate dynamic pile-head displacement compared to field measurements and thereby is likely too conservative for design.

(5) Considering radial inhomogeneity in the soil to simulate installation and loading effects leads to improved simulations of experimentally measured pile response. A single generic value of the inhomogeneity parameter (A = 0.8) was found to provide reasonably accurate predictions in many cases. As a preliminary screening criterion for design purposes, the authors suggest that if the design load frequency is within 20% of the pile–soil resonant frequency, a reduction in radiation damping by a factor of 2 to 2.5 is used, and upper bound analyses (assumed shear wave velocities higher than average measurements) are considered in addition to lower-bound analyses (assumed shear wave velocities lower than average measurements). This criterion can be used in conjunction with available design-oriented formulae in literature such as those provided in Reference [67].

(6) The presence of inhomogeneity leads to gradual diffraction of the waves emitted from the pile and impedes wave propagation towards infinity. In this token, the suppressed frequency dependence of the Winkler springs (especially dashpots) with increasing inhomogeneity is hardly surprising. Interestingly, these effects are not captured by

generic p-y and t-z curves used in practice, as these are not calibrated for dynamic conditions and inhomogeneous soil (let alone presence of double inhomogeneity in the near-pile ground).

(7) Regarding applications to transient problems such as earthquake motions, transient analysis is a complicated problem that lies beyond the scope of this study. Nevertheless, we believe that the reduction in radiation damping observed in harmonic steady-state response will naturally affect transient response. The amount of reduction, however, naturally depends on excitation frequency, number of excitation cycles, number and distribution of natural modes, etc. For instance, loads associated with earthquake shaking are usually of much lower frequency than the loads associated with machine vibrations, so the reduction in response is expected to be lower relative to machine-induced vibrations.

(8) The expressions for stiffness provided in Equations (6)–(9) are calibrated for the range of parameters considered in this paper and probably are not that accurate for extreme conditions such as very soft soils or very slender piles. In the case of very soft soils, it is quite possible that end-bearing piles are used, which would behave differently from our examined configurations. However, to the extent of our knowledge, for L/D greater than 60, such piles are typically not very advisable, as they are prone to creeping.

(9) Regarding inhomogeneity parameter A, we acknowledge there is no consolidated method for establishing a radially inhomogeneous profile around a pile, and the relevant experimental data are very scarce. Furthermore, it would be challenging to infer the A parameter from back-calculating results, because one can get the same results (pile-head settlement, for example) with different combinations of average E_s values and A. However, it is a useful tool if you are trying to make sense of field data that disagree with each other (for example, measured high shear wave velocities but poor performance of a pile). In this context, our results should be interpreted as a proof-of-concept study.

(10) As a final remark, it is noted that the general conclusions are not limited to axisymmetric conditions. In Reference [45], similar conclusions are reached for horizontal pile-head loads. Also, this study is primarily applicable to friction piles. For end-bearing piles, it is possible that the stiffness of the bearing layer is of greater importance for wave radiation and may overshadow radial inhomogeneity. Exploring this effect lies beyond the scope of our work. Finally, the bending of waves toward the pile due to near-field softening has been employed as an ad hoc mechanism for interpreting numerical results in other studies such as Reference [61].

Author Contributions: Conceptualization, G.M. and K.S.; methodology, G.M. and K.S.; software, K.S.; validation, K.S. and G.M.; formal analysis, K.S. and G.M.; investigation, K.S. and G.M.; resources, G.M. and K.S.; data curation, K.S.; writing—original draft preparation, K.S. and G.M.; writing—review and editing, G.M.; visualization, K.S.; supervision, G.M.; project administration, G.M.; funding acquisition, G.M. All authors have read and agreed to the published version of the manuscript.

Funding: This research was funded by the National Science Foundation under U.S.–Japan Collaborative Program (NSF #0000101). George Mylonakis also received partial funding from the University of Patras, through a Caratheodory Grant (B.388), while Konstantinos Syngros received financial support through a PhD scholarship provided by the City University of New York. The authors are grateful for all this support.

Institutional Review Board Statement: Not applicable.

Informed Consent Statement: Not applicable.

Data Availability Statement: The original contributions presented in this study are included in the article. Further inquiries can be directed to the corresponding author.

Conflicts of Interest: Author Konstantinos Syngros is employed by the company Langan Engineering. The remaining authors declare that the research was conducted in the absence of any commercial or financial relationships that could be construed as a potential conflict of interest.

References

1. Mylonakis, G. Elastodynamic model for large-diameter end-bearing shafts. *Soils Found.* **2001**, *41*, 31–44. [CrossRef]
2. Maiorano, R.M.S.; de Sanctis, L.; Aversa, S.; Mandolini, A. Kinematic response analysis of piled foundations under seismic excitations. *Can. Geotech. J.* **2009**, *46*, 571–584. [CrossRef]
3. Dezi, F.; Carbonari, S.; Leoni, G. Kinematic bending moments in pile foundations. *Soil Dyn. Earthq. Eng.* **2009**, *30*, 119–132. [CrossRef]
4. de Sanctis, L.; Maiorano, R.M.S.; Aversa, S. A method for assessing kinematic bending moments at the pile head. *Earthq. Eng. Struct. Dyn.* **2010**, *39*, 1133–1154. [CrossRef]
5. Sica, S.; Mylonakis, G.; Simonelli, A.L. Transient kinematic pile bending in two-layer soil. *Soil Dyn. Earthq. Eng.* **2011**, *31*, 891–905. [CrossRef]
6. Di Laora, R.; Mandolini, A.; Mylonakis, G. Insight on kinematic bending of flexible piles in layered soil. *Soil Dyn. Earthq. Eng.* **2012**, *43*, 309–322. [CrossRef]
7. Di Laora, R.; Mylonakis, G.; Mandolini, A. Pile-head kinematic bending in layered soil. *Earthq. Eng. Struct. Dyn.* **2013**, *42*, 319–337. [CrossRef]
8. Di Laora, R.; Rovithis, E. Kinematic bending of fixed-head piles in nonhomogeneous soil. *J. Geotech. Eng. Div.* **2015**, *141*, 04014126. [CrossRef]
9. Chidichimo, A.; Cairo, R.; Dente, G.; Taylor, C.A.; Mylonakis, G. 1-g experimental investigation of bi-layer soil response and kinematic pile bending. *Soil Dyn. Earthq. Eng.* **2014**, *67*, 219–232. [CrossRef]
10. Martinelli, M.; Burghignoli, A.; Callisto, L. Dynamic response of a pile embedded into a layered soil. *Soil Dyn. Earthq. Eng.* **2016**, *87*, 16–28. [CrossRef]
11. Mucciacciaro, M.; Sica, S. Nonlinear soil and pile behaviour on kinematic bending response of flexible piles. *Soil Dyn. Earthq. Eng.* **2018**, *107*, 195–213. [CrossRef]
12. Di Laora, R.; de Sanctis, L. Piles-induced filtering effect on the foundation input motion. *Soil Dyn. Earthq. Eng.* **2013**, *46*, 52–63. [CrossRef]
13. Anoyatis, G.; Di Laora, R.; Mandolini, A.; Mylonakis, G. Kinematic response of single piles for different boundary conditions: Analytical solutions and normalization schemes. *Soil Dyn. Earthq. Eng.* **2013**, *44*, 183–195. [CrossRef]
14. Di Laora, R.; Grossi, Y.; de Sanctis, L.; Viggiani, G.M.B. An analytical solution for the rotational component of the Foundation Input Motion induced by a pile group. *Soil Dyn. Earthq. Eng.* **2017**, *97*, 424–438. [CrossRef]
15. Poulos, H.G. Analysis of the Settlement of Pile Groups. *Géotechnique* **1968**, *18*, 449–471. [CrossRef]
16. Butterfield, R.; Banerjee, P.K. The elastic analysis of compressible piles and pile groups. *Géotechnique* **1971**, *21*, 43–60. [CrossRef]
17. Anoyatis, G.; Mylonakis, G. Dynamic Winkler modulus for axially-loaded piles. *Géotechnique* **2012**, *62*, 521–536. [CrossRef]
18. Anoyatis, G.; Di Laora, R.; Lemnitzer, A. Dynamic pile impedances for fixed-tip piles. *Soil Dyn. Earthq. Eng.* **2017**, *97*, 454–467. [CrossRef]
19. Novak, M. Dynamic stiffnesses and damping of piles. *Can. Geotech. J.* **1974**, *11*, 574–598. [CrossRef]
20. Blaney, G.W.; Kausel, E.; Roesset, J.M. Dynamic stiffness of piles. In *Proceedings of the 2nd International Conference of Numerical Methods in Geomechanics*; Virginia Polytechnic Institute and State University: Blacksburg, VA, USA, 1975; pp. 1010–1012.
21. Kaynia, A.M.; Kausel, E. *Dynamic Stiffness and Seismic Response of Pile Groups*; Research Report R82-03; Massachusetts Institute of Technology: Cambridge, MA, USA, 1982.
22. Nogami, T. Dynamic group effect in axial response of grouped piles. *J. Geotech. Eng.* **1983**, *109*, 228–243. [CrossRef]
23. Rajapakse, R.K.N.D. Response of an axially-loaded elastic pile in a Gibson soil. *Géotechnique* **1990**, *40*, 237–249. [CrossRef]
24. Wu, G.; Finn, W.D.L. Dynamic elastic analysis of pile foundations using the Finite Element method in the frequency domain. *Can. Geotech. J.* **1997**, *31*, 34–43. [CrossRef]
25. Boulanger, R.W.; Curras, C.J.; Kutter, B.L.; Wilson, D.W.; Abghari, A. Seismic soil-pile-structure interaction experiments and analyses. *J. Geotech. Geoenviron. Eng.* **1999**, *125*, 750–759. [CrossRef]
26. Guo, W.D. Vertically loaded single piles in Gibson soil. *J. Geotech. Geoenviron. Eng.* **2000**, *126*, 189–193. [CrossRef]
27. Kim, S.; Stewart, J.P. Kinematic soil-structure interaction from strong motion recordings. *J. Geotech. Geoenviron. Eng.* **2003**, *129*, 323–335. [CrossRef]
28. Poulos, H.G. Pile behaviour—Theory and application. *Géotechnique* **1989**, *39*, 365–415. [CrossRef]

29. Novak, M. Piles under dynamic loads: State of the art. In Proceedings of the 2nd International Conferences on Recent Advances in Geotechnical Earthquake Engineering and Soil Dynamics, St. Louis, MI, USA, 11–15 March 1991; pp. 2433–2456.
30. Pender, M. Aseismic pile foundation design analysis. *Bull. N. Z. Natl. Soc. Earthq. Eng.* **1993**, *26*, 49–160. [CrossRef]
31. Gazetas, G.; Mylonakis, G. *Seismic Soil-Structure Interaction: New Evidence and Emerging Issues*; Emerging Issues Paper, Geotechnical Special Publication No 75; ASCE: Reston, VA, USA, 1998; pp. 1119–1174.
32. Randolph, M.F. Science and empiricism in pile foundation design. *Géotechnique* **2003**, *54*, 847–874. [CrossRef]
33. Crispin, J.J.; Mylonakis, G. Simplified models for axial static and dynamic analysis of pile foundations. In *Analysis of Pile Foundations Subject to Static and Dynamic Loading*; CRC Press: Boca Raton, FL, USA, 2021; pp. 131–184.
34. Di Laora, R.; Rovithis, E. Design of piles under seismic loading. In *Analysis of Pile Foundations Subject to Static and Dynamic Loading*; CRC Press: Boca Raton, FL, USA, 2021; pp. 269–300.
35. Poulos, H.G. Modified calculation of pile-group settlement interaction. *J. Geotech. Eng.* **1988**, *114*, 697–706. [CrossRef]
36. Bateman, A.H.; Crispin, J.J. Theoretical t-z curves for radially inhomogeneous soil. *DFI J. J. Deep Found. Inst.* **2020**, *14*, 1–8.
37. Novak, M.; Sheta, M. Approximate approach to contact effects of piles. In *Dynamic Response of Pile Foundations: Analytical Aspects*; ASCE: New York, NY, USA, 1980; pp. 53–79.
38. Veletsos, A.S.; Dotson, K.W. Impedances of soil layer with disturbed boundary zone. *J. Geotech. Eng.* **1986**, *112*, 363–368. [CrossRef]
39. Han, Y.C.; Sabin, G.C.W. Impedances for radially inhomogeneous viscoelastic soil media. *J. Eng. Mech. Div.* **1995**, *121*, 939–947. [CrossRef]
40. Michaelides, O.; Gazetas, G.; Bouckovalas, G.; Chrysikou, E. Approximate non-linear dynamic axial response of piles. *Géotechnique* **1998**, *48*, 33–53. [CrossRef]
41. El-Naggar, M.H. Vertical and torsional soil reactions for radially inhomogeneous soil layer. *Struct. Eng. Mech.* **2000**, *10*, 299–312. [CrossRef]
42. Bateman, A.H.; Mylonakis, G. p-y curves for piles in radially inhomogeneous soil. In Proceedings of the 17th Danube European Conference on Geotechnical Engineering (17DCGE), Bucharest, Romania, 7–9 June 2023.
43. Karatzia, X.; Papastylianou, P.; Mylonakis, G. Horizontal soil reaction of a cylindrical pile segment with a soft zone. *J. Eng. Mech.* **2014**, *140*, 04014077. [CrossRef]
44. Fu, P.; Wu, J.; Jia, J.; Yi, E.; Wang, K.; Zhang, Z. Dynamic response of saturated layered soil around defective piles and its application in engineering testing. *Soil Dyn. Earthq. Eng.* **2025**, *194*, 109391. [CrossRef]
45. Syngros, C. Seismic Response of Piles and Pile-Supported Bridge Piers Evaluated Through Case Histories. Ph.D. Dissertation, The City University of New York, New York, NY, USA, 2004.
46. Mattes, N.S. The influence of radial displacement compatibility on pile settlement. *Géotechnique* **1969**, *19*, 157–159. [CrossRef]
47. Marques, J.M.; Owen, D.R.J. Infinite elements in quasi-static materially nonlinear problems. *Comput. Struct.* **1984**, *18*, 739–751. [CrossRef]
48. Kellezi, L. Local transmitting boundaries for transient elastic analysis. *Soil Dyn. Earthq. Eng.* **2000**, *19*, 533–547. [CrossRef]
49. Price, T.E. Numerically exact integration of a family of axisymmetric finite elements. *Commun. Numer. Methods Eng.* **2003**, *19*, 253–261. [CrossRef]
50. Syngros, C.; Mylonakis, G.; Price, T. Influence of soil heterogeneity on dynamic response of deep foundations. In Proceedings of the 5th GRACM, International Congress on Computational Mechanics (8 pages on CD-ROM), Limassol, Cyprus, 29 June–1 July 2005.
51. Kim, Y.S. Dynamic Response of Structures on Pile Foundations. Ph.D. Dissertation, The University of Texas at Austin, Austin, TX, USA, 1987.
52. Zheng, C.; Mylonakis, G.; Kouretzis, G. Inertial and kinematic response of laterally loaded piles: Sensitivity of elastodynamic continuum solutions to key assumptions. *Soil Dyn. Earthq. Eng.* **2024**, *178*, 108485. [CrossRef]
53. El-Sharnouby, B.; Novak, M. Stiffness constants and interaction factors for vertical response of pile groups. *Can. Geotech. J.* **1990**, *27*, 813–822. [CrossRef]
54. El-Marsafawi, H.; Kaynia, A.M.; Novak, M. *Interaction Factors and the Superposition Method for Pile Group Dynamic Analysis*; Geotechnical Research Center Report GEOT-1-92; The University of Western Ontario: London, ON, Canada, 1992.
55. O'Neill, M.W.; Ghazzaly, O.I.; Ha, H.B. Analysis of three-dimensional pile groups with nonlinear soil response and pile-soil-pile interaction. In Proceedings of the 9th Annual Offshore Technology Conference, Houston, TX, USA, 2–5 May 1997; Paper No. OTC 2838.
56. Bevington, P.R.; Robinson, D.K. *Data Reduction and Error Analysis for the Physical Sciences*; McGraw Hill: New York, NY, USA, 1992.
57. Pak, R.Y.S.; Ji, F. Rational mechanics of pile-soil interaction. *J. Eng. Mech.* **1993**, *119*, 813–832. [CrossRef]
58. Roesset, J.M. Stiffness and damping coefficients of foundations. In *Proceedings ASCE, Geotechnical Engineering Division, National Convention*; ASCE: Reston, VA, USA, 1980; pp. 1–30.
59. Gazetas, G.; Fan, K.; Tazoh, T.; Shimizu, K.; Kavvadas, M.; Makris, N. Seismic response of soil-pile-foundation-structure systems: Some recent developments. In *Piles Under Dynamic Loads*; Special Publication No. 34; ASCE: Reston, VA, USA, 1992.
60. Blaney, G.W.; Muster, G.L.; O'Neill, M.W. Vertical vibration test of a full-scale pile group. In *Dynamic Response of Pile Foundations-Experiment, Analysis and Observation*; Nogami, T., Ed.; Geotechnical Special Publication No. 11; ASCE: Reston, VA, USA, 1987.

61. Gazetas, G. Foundation Vibrations. In *Foundation Engineering Handbook*; Springer: New York, NY, USA, 1991; pp. 553–593.
62. Li, Z.; Jin, N.; Zhang, C.; Zhang, Z.; Wu, W. Vertical vibration of pipe piles in construction-induced inhomogeneous saturated soil. *Ocean Eng.* **2025**, *341*, 122750. [CrossRef]
63. Guin, J. Advanced Soil-Pile-Structure Interaction and Nonlinear Behavior. Ph.D. Dissertation, State University of New York, Buffalo, NY, USA, 1997.
64. El Sharnouby, B. Static and Dynamic Behavior of Pile Groups. Ph.D. Dissertation, The University of Western Ontario, London, ON, Canada, 1984.
65. Janes, M.C.; Novak, M. Pile Group response to large lateral loads. In *Proceedings of the 42nd Canadian Geotechnical Conference*; Canadian Geotechnical Society: Surrey, BC, Canada, 1989; pp. 216–222.
66. Mylonakis, G.; Gazetas, G. Vertical vibrations and additional distress of grouped piles in layered soil. *Soils Found.* **1998**, *38*, 1–14. [CrossRef]
67. Stewart, J.P.; (Project Director) NEHRP Consultants Joint Venture. *Soil-Structure Interaction for Building Structures*; Report NIST GCR-12-917-21; National Institute of Standards and Technology: Gaithersburg, MD, USA, 2012.

Disclaimer/Publisher's Note: The statements, opinions and data contained in all publications are solely those of the individual author(s) and contributor(s) and not of MDPI and/or the editor(s). MDPI and/or the editor(s) disclaim responsibility for any injury to people or property resulting from any ideas, methods, instructions or products referred to in the content.